PROCEEDINGS, 47th Workshop on Geothermal Reservoir Engineering
Stanford University, Stanford, California, February 7-9, 2022
SGP-TR-223

Evaluation of Hammer Drillbit Performance in Rotary Percussive Drilling

Roman J. Shor[1,*], Shanti Swaroop Kandala[1], Ajesh Trivedi[1], Juan De la Fuente Valadez[1], An Mai[1], and Alex Vetsak[2]

[1] Department of Chemical and Petroleum Engineering, University of Calgary, Calgary, Alberta, Canada
[2] Eavor Technologies, Inc, Calgary, Alberta, Canada

*roman.shor@ucalgary.ca

Keywords: rotary percussive drilling, hammer bit, bit performance index, hard rock drilling

ABSTRACT

Percussive and rotary percussion drilling (RPD) has been deployed extensively in shallow drilling applications in mining operations to improve the rate of penetration (ROP) through hard rock, such as granite. However, for deep drilling, where depths exceed 3 km, through hard rocks, the limited understanding of rotary percussion drilling tools, fluid hammers, and drill bits, has been a major drawback. Field experience and past experimental work have shown a non-linear relationship between bit RPM, hammer frequency and rate of drilling and the incidence of damaging vibrations. Therefore, it is important to understand the coupling between rotary and axial motion of the hammer bits to extend bit life and improve the rate of penetration. We present a novel approach to compare and validate the effectiveness of different hammer bits and operation in RPD by introducing a metric we call the Bit Performance Index (BPI). The BPI uses the shape and layout of inserts on a bit face and the relationship between bit RPM and hammer frequency to evaluate the overlap between hammer blows, and thus drilling efficiency. The two main applications of the BPI are to compare and evaluate the configuration and layout of diamond inserts on hammer bits and then to obtain the optimal operating parameters during drilling with a given bit. The most important aspect of the BPI is that it uses only the drill bit geometry, bit RPM, and hammer frequency with ROP and delivered energy as the performance metric. The BPI is first validated using data collected with a laboratory-scale experiment and then validated with field data from shallow test wells drilled in Europe and North America.

The reward function used in the current work is inspired by those used in machine learning contexts, such as Q-learning. Usually, reward functions either reward or penalize an action depending on the desired outcome, and here the reward function considers the overlap between impact locations of the individual inserts on a hammer bit face. In this work, the reward function is based on the impact location of the current hit with respect to a previous impact. If the current impact is on the edge of any previous impact, it would lead to greater rock destruction due to higher stress load and thus is rewarded. However, if it is on the same location as any previous impact, it would lead to less rock destruction due to lower axial force transmission and lower stress and thus penalized. The reward function is combined with the geometry of the hammer bit and yields an overall reward for a particular rpm and hammer frequency. This approach is validated with a single insert experiment to evaluate rock failure as a function of impact overlap. An experimental rig has been developed which applies an identical amount of energy to every impact. Diamond percussion insert(s) with different shapes are used to impact granite and impact size, force, and coefficient of restitution are measured. The BPI is also compared with field data showing preliminary agreement. The proposed metric will provide insights into the drilling performance, especially the bit wear, and help in obtaining optimal combinations of the hammer frequency and the bit RPM.

1. INTRODUCTION

Deep drilling for geothermal resources away from geologic hot spots and tectonic plate boundaries necessitates the drilling of boreholes through basement rock comprised of metamorphic and granite rock. Drilling rates through granite have historically been quite low (up to 10 m per hour) using impregnated diamond bits rotating at high speeds using downhole turbines or with air-hammer percussive and rotary percussive drillbits. To enable economic development of deep geothermal resources, a step change in drilling technology is necessary to improve drilling rates and survival of drillbits significantly. One promising technology integrates fluid hammers with rotary percussive drillbits. Typical rotary bits have positive relationships between rotary torque, weight-on-bit and rate of penetration, where an increase in either torque or weight-on-bit results in an increase in rate of penetration until the founder point is reached (Dupriest and Koederitz, 2005). Rotary percussive drillbits do not have the same relationship and instead exhibit a non-linear relationship between rotary rate, hammer rate, hammer power and rate of penetration. To understand these phenomena, the relationship between the layout and shape of the diamond inserts on the drillbit face and operation conditions is desired. In this paper, we propose one such metric, which we call the Bit Performance Index (BPI), based on the layout and shape of the diamond inserts combined with the angular distance between blows of the hydraulic hammer as the bit rotates.

This paper is presented as follows:

- A brief literature review and motivation is presented in Section 2.
- The bit performance index (BPI) is derived in Section 3 from the Gabor wavelet and is demonstrated on a single cutter, a simple three cutter bit and a complex field bit.
- The BPI is compared with preliminary results from a single cutter experimental setup in Section 4.
- Field data from a rotary percussive field test is compared with the BPI in Section 5.
- The potential of the BPI for rotary percussive drilling and the next steps are discussed in Section 6.

2. LITERATURE REVIEW

Before modern rotary drilling techniques were invented in the early 1900s, deep wells were drilled with percussive tools (Kop ey, 2007). Air hammer technologies have been in use in shallow applications, particularly in the mining sector, for decades. Hydraulic hammers have been recently explored for deeper applications, both in the mining and petroleum sectors (Melamed et al., 2000). In the mid-1930s, improvements in rotary rigs led to a reduction of popularity of percussion drilling and the rise of the modern rotary drilling rig. In the 1980s, continued evolution of tools and designs of bottom hole assemblies (BHA) brought renewed attention to RDP. Further improvement in bit design resulted in impregnated diamond and polycrystalline diamond compact inserts to improve cutting structure and penetration rates (Sapinska-Sliwa et al, 2015). Rotary drillbits remain the workhorse of the drilling industry.

For rotary drillbits, significant work exists that explores drillbit design, drillbit modelling and optimization of drilling operations based on the understanding of the drillbit and BHA (Detournay and Defourny, 1992; Gerbaud et al., 2006; Richard et al., 2007; Detournay et al., 2008; Perneder et al., 2012). In these, and other, studies, a numerical model of the bit is derived from abstracting cutting surfaces as blades, and is then used to evaluate drilling efficiencies, induced vibrations, including axial and torsional vibrations, and optimization of drilling parameters to improve rate of penetration.

Rock failure mechanics for rotary percussive bits have been explored at length (Han et al., 2005; Bu et al., 2009; Depouhon et al., 2015), however, an easy-to-use metric to evaluate overall bit performance and propose optimal operating parameters has not yet been developed, as has been for rotary bits. In machine learning and optimization contexts, reward or objective functions have been used extensively, however, formulation of these functions is critical to find global, rather than just local, minima or maxima.

3. THE BIT PERFORMANCE INDEX

In this section, we present the mathematical formulation for the Bit Performance Index. In many optimization and path planning algorithms, an objective function is formulated to generate an optimization surface which can be utilized by an optimization algorithm such as gradient descent.

A rotary percussive drillbit uses shaped diamond inserts, which may have a spherical or arbitrary shape, laid out in a specific pattern on a bit body. The bit itself rotates at rotary rate, ω, and exerts an oscillating axial force, $F_a \approx A_o + A \sin \omega_a t$, or weight on bit, on the formation. ω, ω_a, A_o and A are taken to be constants, where ω_a is the axial oscillation frequency, A_o is steady-state axial force and A is the amplitude of the oscillating force.

3.1 Considering a single insert

Between maximum and minimum axial force, an insert on a drillbit will rotate an angular distance $\delta = \omega r \Delta t$ where r is the distance from the insert from the center of the bit and Δt is the time between hammer impacts. We postulate that maximum rock failure will occur when the subsequent maximum axial force is applied at the edge of the crater created by the prior maximum axial force. Thus, we want an optimization function that is positive value along the edge of a circular region, negative in the middle and zero far away from the crater.

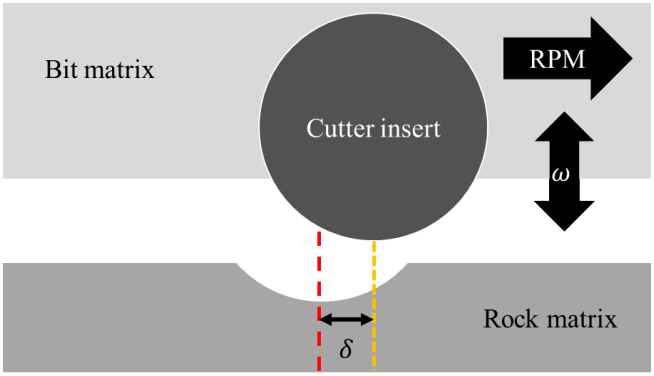

Figure 1: An abstraction of the bit matrix, a dome shaped cutter, the indentation from the prior blow and the distance travelled, δ, between blows.

To achieve this, we use a one-dimensional Gabor wavelet

$$f(x) = e^{(x-x_o)^2/a^2} e^{-ik_o(x-x_0)}$$

If we have $a = 1$, $x_0 = 0$ and $k_0 = 1$, we have a function that suits our needs and contains additional information in the complex form, as shown in Figure 2. In the complex domain, an impact on the right side of the previous blow is positive, and on the left, negative. If motion is assumed to be from left to right, the complex component of the Gabor wavelet may be used to indicate if the next blow is occurring on the leading or trailing edge of a prior blow.

This wavelet may be multiplied with a function describing the function of the individual insert. We will describe a spherical insert; however, suitable shape functions may be derived for an arbitrarily shaped insert. These functions should be piecewise continuous, but do not need to be differentiable. For a spherical insert, we may use $y = \sqrt{r^2 - x^2} - (r - \zeta)$, where r is the radius of curvature of the insert and ζ is the standoff of the insert from the bit matrix. To find the **bit performance index** (BPI), the shape function and the Gabor wavelet are multiplied, as shown in Figure 2.

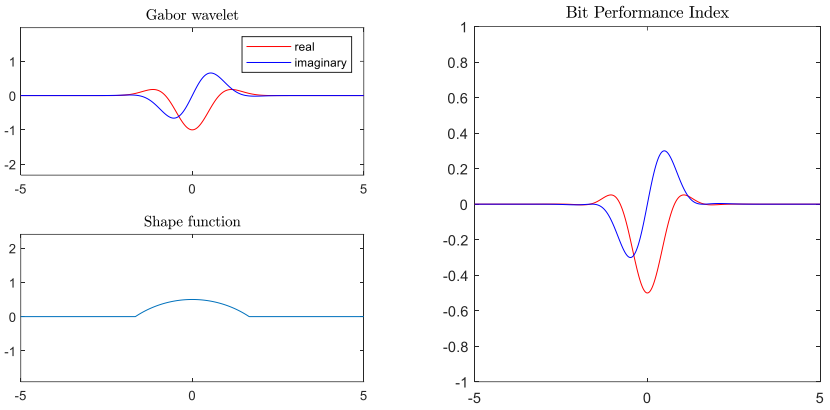

Figure 2: (top left) The Gabor wavelet with the real part plotted in blue and the imaginary part plotted in red. The x-axis may be taken as δ and the y-axis as the value of an objective function. (bottom left) a shape function for a spherical insert with $r = 3$ and $\zeta = 0.5$. (right) the resulting bit performance index.

A three-dimensional form of the bit performance index may be obtained by rotating the wavelet and shape functions around the y-axis, as shown in Figure 3. Special care must be taken to obtain the proper complex form of the wavelet if insert motion is to be assumed to be from the negative towards the positive x-domain.

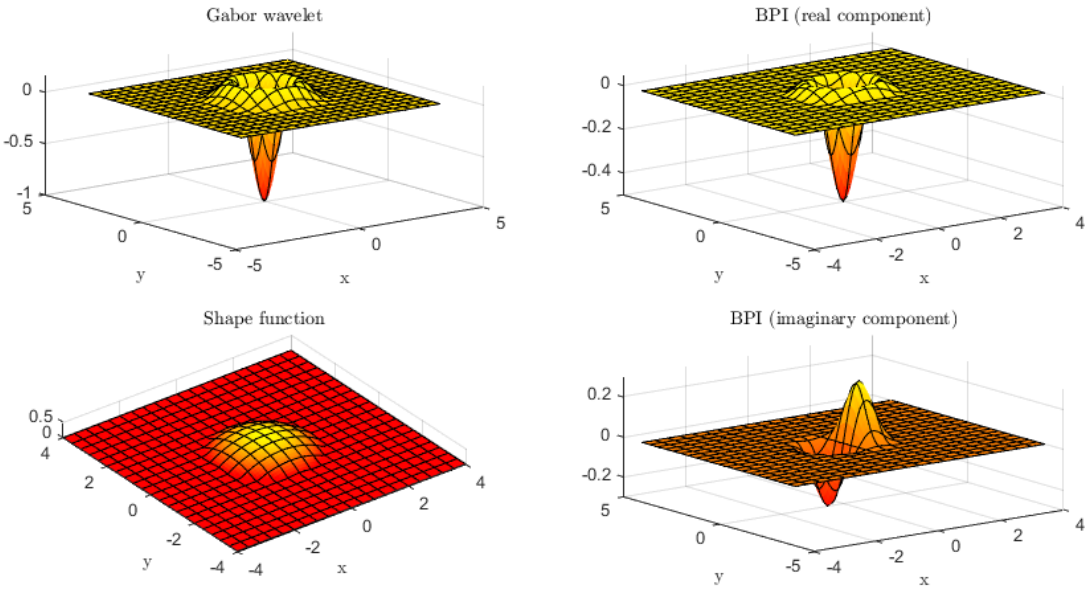

Figure 3: (top left) The real component of the 3-D Gabor wavelet. (bottom left) a shape function for a spherical insert with $r = 3$ and $\zeta = 0.5$. (top right) the real component and (bottom right) imaginary component of the resulting bit performance index.

On the scale of a single cutter, the effect of overlap between hammer blows may now be quantified. The validity of the negative and positive real regions is validated using a single insert experiment which will be described in the next section.

3.2 Considering a full bit

The single insert formulation of the BPI may be extended to describe a full bit. In the previous subsection, the insert was assumed to be at (0,0). In a full bit, each insert is located at a particular position (x_i, y_i) or, more generally, (r_i, θ_i) where r_i is the radial distance of the

insert to the center of the bit and θ_i is the angular distance from some arbitrary zero-angle. Thus, the shape function may be simply assembled by summing the shape functions of the i inserts placed at locations (r_i, θ_i). Similarly for the Gabor wavelets. The complex component must be rotated by θ_i to take the angular position of the insert into account. For a simple three insert bit, the shape function and the real and imaginary components of the Gabor wavelet function are shown in Figure 4.

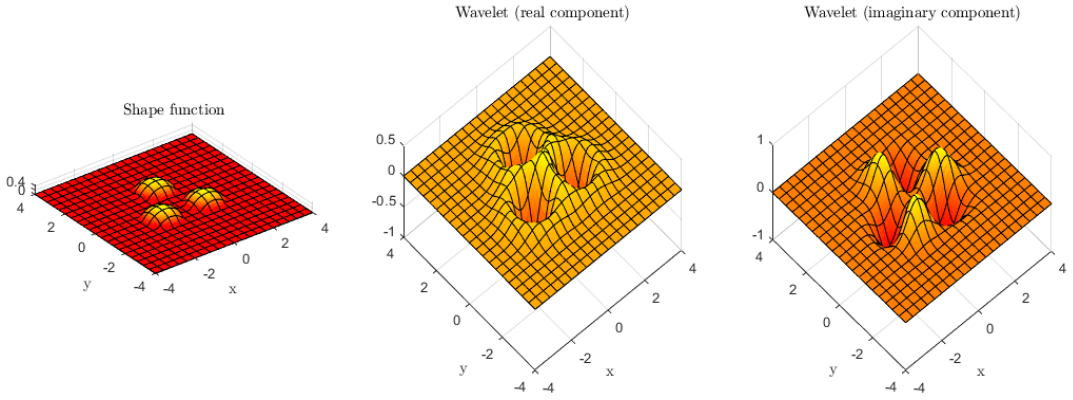

Figure 4: (left) The shape function for a three-cutter bit with three spherical inserts with $r = 4$ and $\zeta = 0.5$. (center) the real component and (left) imaginary component of the 3-D wavelet.

A full bit rotates with a specific RPM, ω_b, and a hammer operates at a specific frequency, f. For a given combination of (ω_b, f) the angular displacement of an insert may be calculated:

$$\delta = \frac{\omega_b}{f} r$$

Thus, for the three-insert bit, if the hammer frequency is taken to be 1 Hz, the BPI may be calculated by summing the product of the rotated shape function and the wavelet function, giving the curve shown in Figure 5. This curve may be interpreted as:

- At multiples of 20 RPM, the bit rotates an additional 1/3 of a rotation, aligning the hammer blow with the location of the previous hammer blow.
- At multiples of 20 RPM starting at 10 RPM, the bit rotates an additional 1/6th of a rotation, allowing it to impact the area between the prior impacts, along the edge of the impact zones.

This plot may lead to the following interpretation: for a hammer operating once per second, rotating at one revolution per second (or 60 RPM) is not a good operating window as the hammer blow will continue to excavate further in the same locations, leading to a potential pattern at the bit face. Operating at 50 or 70 RPM allows for the hammer blows to be distributed more evenly and each blow will land at the edge of a previous blow, potentially concentrating destructive energy.

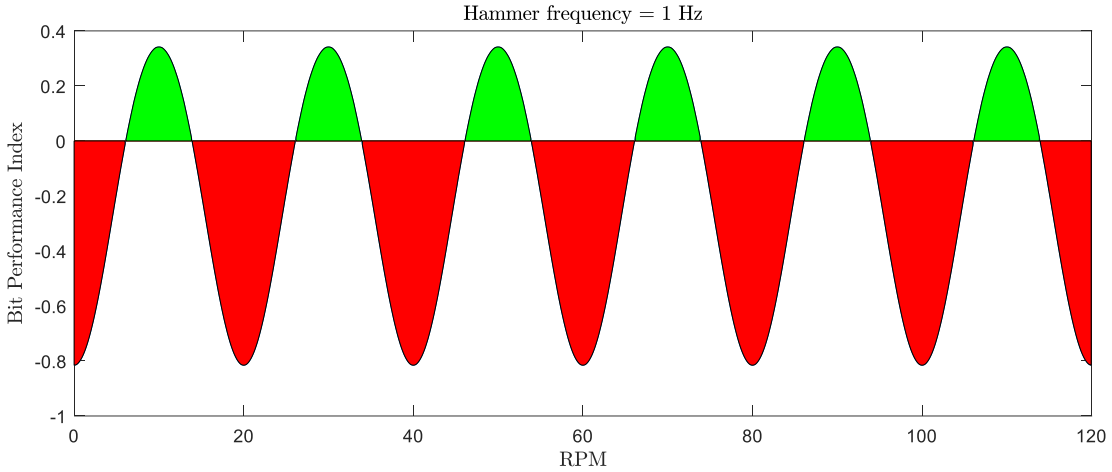

Figure 5: (left) The Bit Performance Index for a three-insert bit, with the hammer operating at 20 Hz.

A complex field drillbit may be considered in the same way. Consider, for example, the drillbit in Figure 6. This is a drillbit designed for hammer drilling that was tested in a test well in late 2020 for drilling of granite. The inserts were quite large and protruded a significant amount from the bit face.

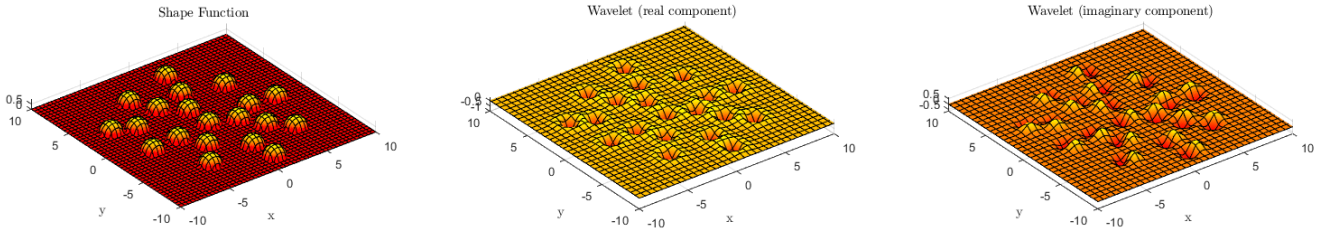

Figure 6: (left) the shape function for a field drillbit (center) the real component and (left) imaginary component of the 3-D wavelet.

The following observations may be deduced from the calculated BPI, shown in Figure 7:

- For a wide range of RPMs and hammer frequency combinations, a positive BPI is computed. The real component indicates that there is partial overlap with prior impacts for large bands of RPM, while the imaginary component shows that either the trailing or leading edge of the prior impact can predominantly be impacted on the subsequent blow.
- Given an operating frequency for the fluid hammer, there are wide ranges of RPM where BPI is positive. For regions with a negative BPI, the BPI may be made positive by increasing or decreasing bit RPM by 10 – 15%.
- For each range of positive BPI, the lower RPM results primarily in trailing edge impacts, while the higher RPM in the range results in leading edge impacts.

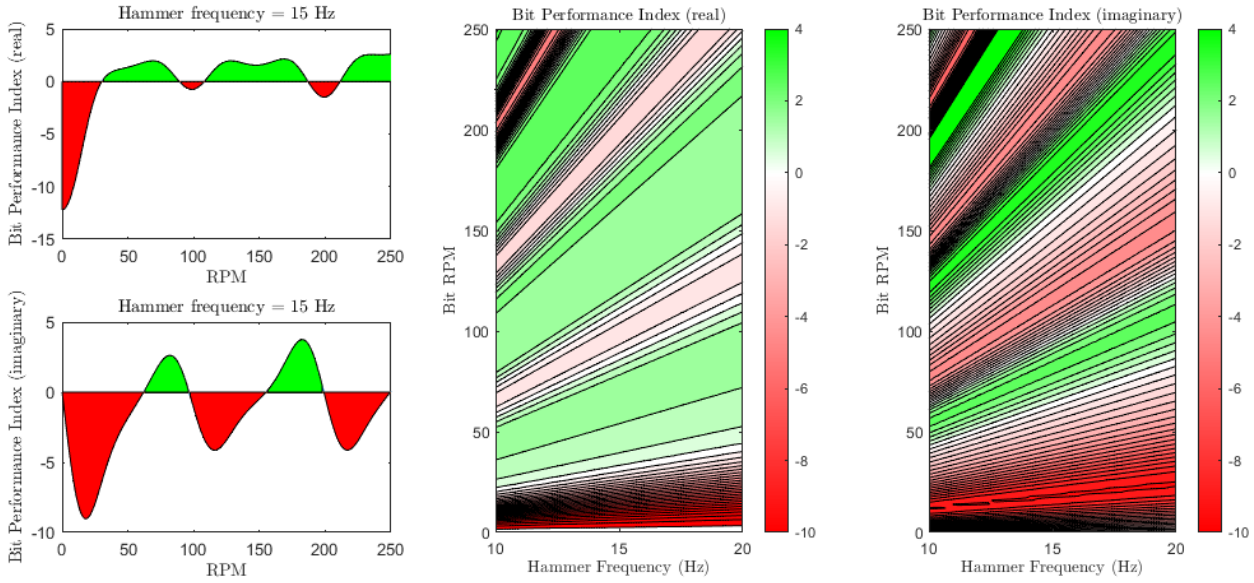

Figure 7: (top left) real and (bottom left) imaginary components the BPI for a hammer frequency of 15 Hz and (center) real and (right) imaginary components the BPI for RPMs in the range of 0 to 250 and hammer frequencies in the range of 10 to 20 Hz.

4. EXPERIMENTAL VALIDATION

A single cutter drop test experimental rig was designed to validate the BPI. As the BPI postulates that an impact on the edge of a prior impact would result in the greatest rock removal (and thus higher penetration rate), the experiment was designed to deliver an impact with a target of 100 Joules to a field scale insert resting on a piece of granite. The rig consists of a rail guide to deliver a mass in freefall to an insert holder. Force and displacement are measured and allow for the calculation of depth of cut (or indentation depth), acceleration, recoil and force of impact. A schematic of the experimental setup is shown in Figure 8. A full description of the experiment rig, calibration of the system and subsequent calculations will be described in a future publication, however, preliminary results are included as an initial validation of the BPI. Mineral compositions of granite rock used in the experiments and its geomechanical properties are summarized in Table 1 and Table 2. Minerology obtained from XRD, shows a significant amount of feldspar with a small quantity of quartz.

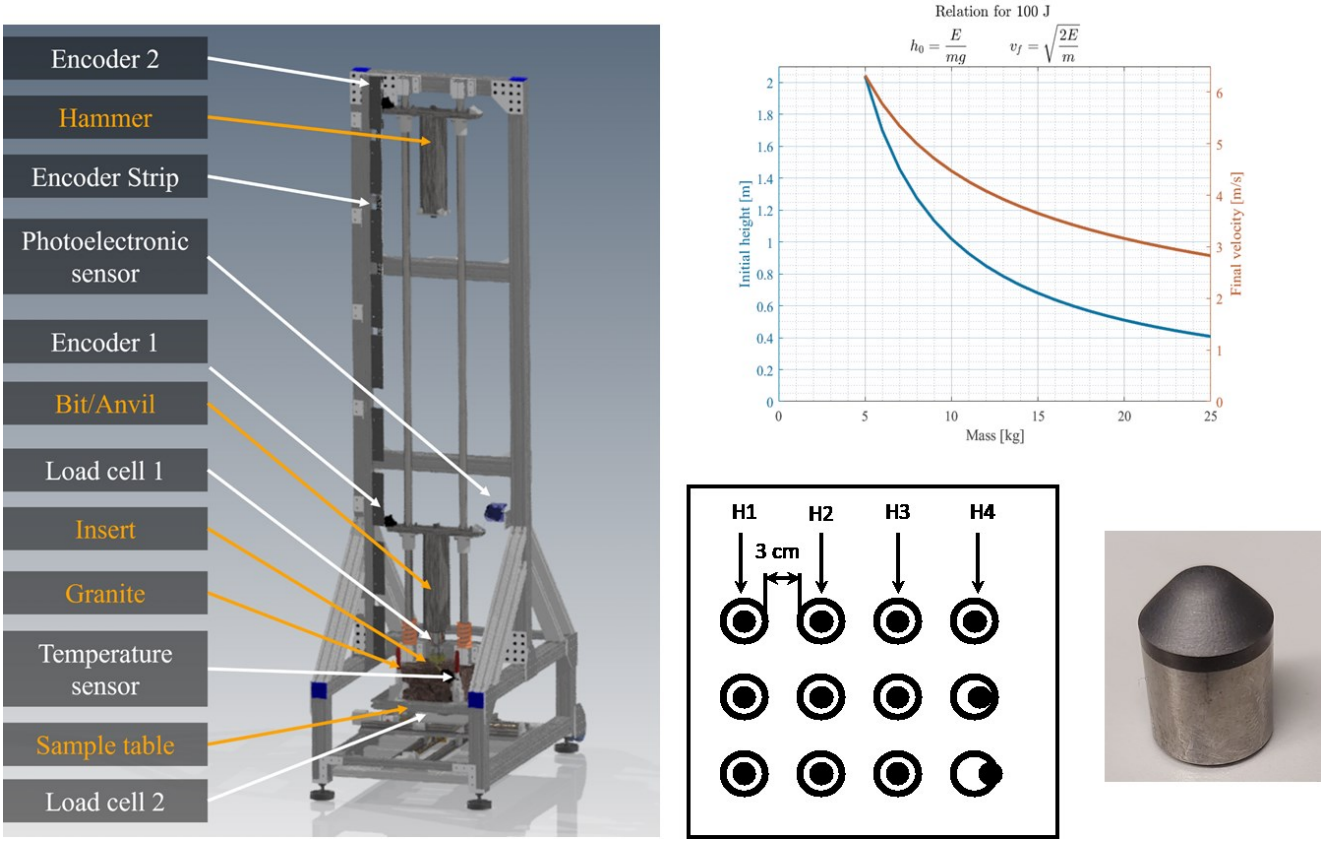

Figure 8: (left) a schematic of the experimental setup, (top right) the necessary mass and heights to deliver 100 J of energy to the insert, (middle bottom) layout of impact sites on a piece of granite and (bottom right) the insert used for experiments.

Table 1: Minerology of Granite used in the Experiments

Mineral Name	Chemical Compound	Concentration (wt%)
Plagioclase feldspar	$(CaNa)Al_2Si_2O_8$	49.5
Potassium feldspar	$KAlSi_3O_8$	4.6
Diopside	$CaMgSi_2O_6$	21.7
Enstatite	$Mg_2Si_2O_6$	14.2
Quartz	SiO_2	5.7
Phlogopite	$K(Mg,Fe)_3(AlSi_3O_{10})(OH)_2$	2.1
Hornblende	$Ca_2(Mg,Fe^{2+})_4Al(Si_7Al)O_{22}(OH)_2$	1.7
Kaolinite	$Al_2Si_2O_5(OH)_4$	0.5

Table 2: Granite Geomechanical Properties

Compressive Strength (MPa)	91.08
Static Poisson's Ratio	0.143
Static Young's Modulus (GPa)	45.06
Static Bulk Modulus (GPa)	21.04
Static Shear Modulus (GPa)	19.71

A preliminary set of experiments were performed to determine if the setup would generate the necessary data, as well as to evaluate the proper metrics to use to compare the impact experiment with the BPI. The weight was released from the same height, and force was measured for each experiment. The following experiments were run:

1. Four impacts on the same location
2. Three impacts on the same location, followed by one offset by approximately one half the radius of the impact crater.
3. Three impacts on the same location, followed by one offset by approximately the radius of the impact crater.

A laser encoder was used to measure the distance penetrated in the rock with each impact. In Figure 9, the difference between initial and final laser position is measured as depths of cut (DOC) after calibrations (top) and corresponding force required is recorded (bottom).

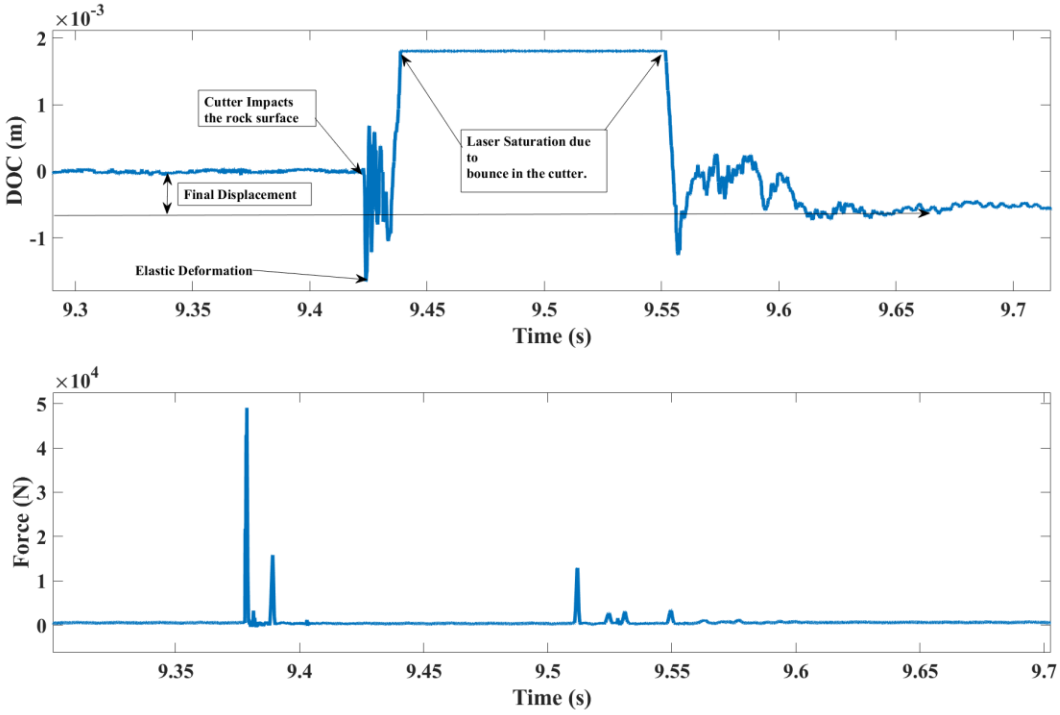

Figure 9: Sample results from the experimental setup. The depth of cut (in meters) is shown in the top subplot and the force (in Newtons) is shown in the bottom subplot.

Variance in the results obtained for a series of experiments is shown in Figure 10, where first three impacts are at the center of the crater to (1) excavate a crater and (2) evaluate the trend in resultant depth and force for subsequent impacts. Next, the fourth impact is aligned in one of three locations: at $r = 0, r = \frac{1}{r_i}$ and $r = r_i$, or equivalently, aligned in the center of the crater, half way to the edge of the crater, and at the edge of the crater. To normalize the changes in impact force, the increase in the depth of the crater (the depth of cut) is normalized by the force of the impact, which can be translated into process efficiency in terms of force required to penetrate through the rock in terms of measured depths of cut.

Preliminary results do show a trend consistent with the trend postulated by the BPI. These are shown in figure 10:

1. Experiments with impacts at the center depict neutral to negative effect on efficiency with constant or higher energy requirements to penetrate through the rock. (labeled 'Center' in Figure 10).
2. Impacts away from the edge but still in the crater allow for elongation of the crater with lower energy requirements as compared with previous impacts at the center. (labeled 'Center-Edge' in Figure 10).
3. Impacts on the edge of the create cause greater failure and thus needed the least energy per unit of evacuation. (labeled 'Edge' in Figure 10).

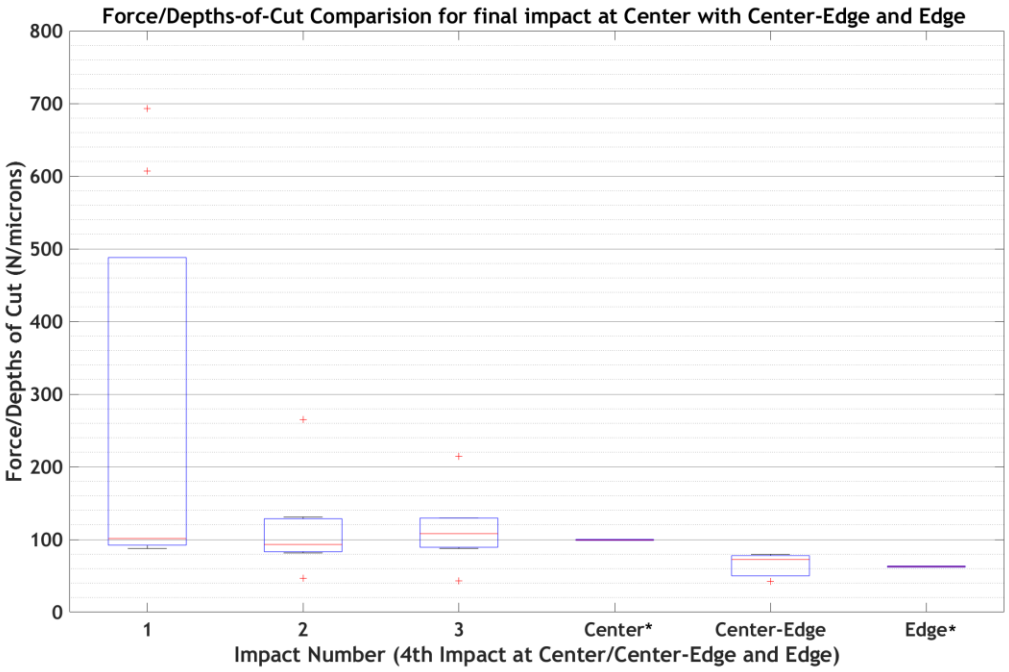

Figure 10: Comparison of energy requirements (Force/Depths of Cut) for final Impact at Centre, between Centre and Edge, and Edge. (* = Limited data points)

5. COMPARISON WITH FIELD DATA

Field trials conducted in 2020 with a variety of rotary percussive hammer bits and fluid hammers were conducted in granite rock at depths ranging from 1,000 to 3,000 feet. Several of these runs included experiments where surface RPMs had large ranges, which allowed the BPI to evaluated, with rate of penetration (ROP) as the initial metric. Rotary-percussive mechanical specific energy (MSE) is a more desirable metric, however, for simplicity in this paper, just ROP is considered. Rotary-percussive MSE will be the subject of a future paper as hammer efficiency and energy radiation must be considered to attain a useful metric. The cutter layout and real and imaginary components of the wavelet function for the drillbit used is shown in Figure 11.

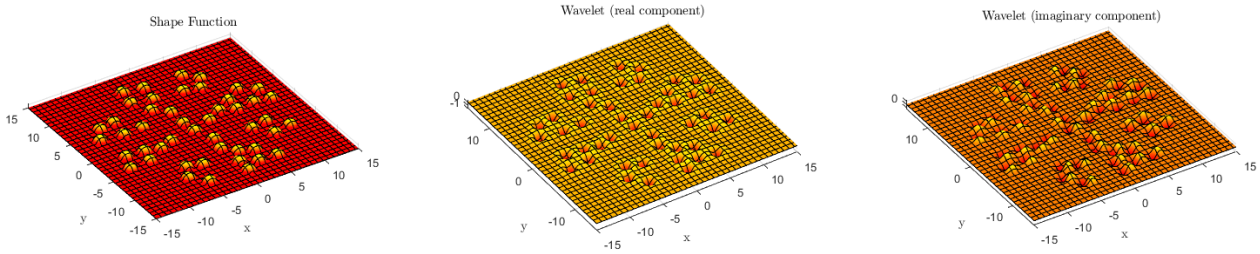

Figure 11: The insert layout (left) and the real (center) and imaginary (right) components of the wavelet function for the field drillbit.

For the bit run presented here, a range of flow rates, and thus a range of hammer frequencies, and a range of surface RPM set points were used. As this was a shallow well, it is assumed that surface and downhole RPM is the same, and as there were no significant oscillations in rotary torque, no significant torsional vibrations were observed. Significant changes in flow rate not only affected hammer frequency, but also hammer power, which is not considered by the BPI, so this should be taken in consideration when comparing results: an increase in hammer power should result in an increase in drilling rate. The BPI for a hammer rate of 15 Hz, the overall BPI and the ROP for a range of RPM and hammer frequency combinations observed in the field data is shown in Figure 12. One immediate observation is that there is not a consistent increase in penetration rate with an increase in hammer frequency (or energy delivery by the fluid hammer), nor with bit RPM. Comparing the BPI prediction with the ROP plot, the following observations may be made:

- High ROP is observed at lower RPM, particularly around 20 and 40 RPM and a hammer frequency between 15 and 25 Hz. For these same ranges of parameters, BPI is calculated to be greater than zero.
- Lower ROP is observed at higher RPMs, greater than 50, and higher hammer frequencies, above 15 Hz. This, in general, corresponds to the area where BPI is around zero.
- For a hammer frequency of 13 – 14 Hz, higher ROPs are visible between 40 and 60 RPM, which correspond to higher BPI values.
- Prediction of negative BPI could not be directly evaluated in this dataset as the drillbit has an overall positive BPI for a wide range of RPMs.

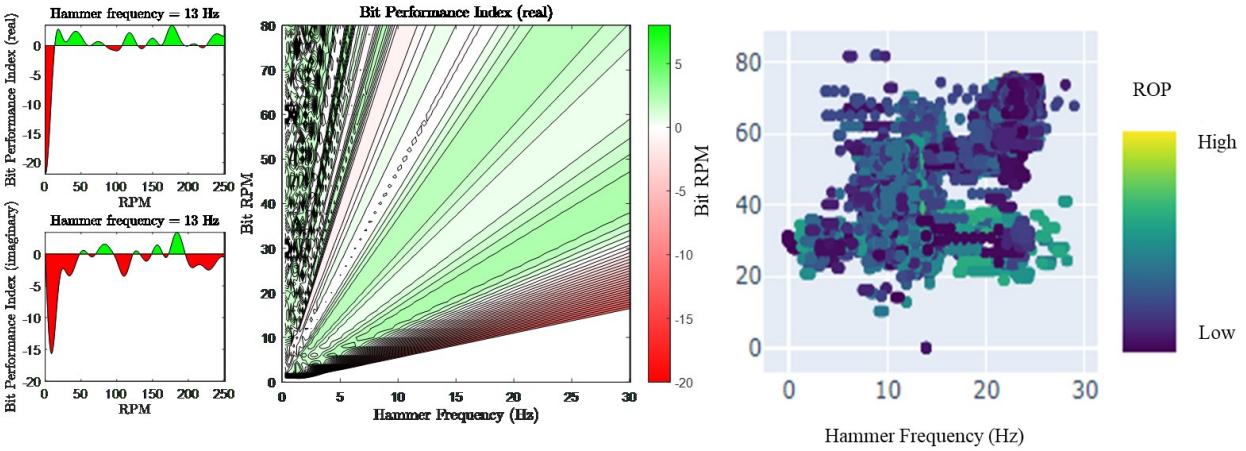

Figure 12: The real and imaginary components of BPI for at hammer frequency of 13 Hz (left), the real component of the BPI vs RPM and hammer frequency (center) and the observed ROP for a range of bit RPM and hammer frequency values from field data (right).

While rudimentary, this preliminary comparison between field data and the BPI indicates agreement. Future work includes evaluation of additional datasets and use of the mechanical specific energy instead of penetration rate as a comparison metric.

6. DISCUSSION AND POTENTIAL OF THE BPI

The bit performance index proposed in this paper provides a simple metric, based on the geometry of the drillbit and operating parameters, to understand the operational potential of a particular drillbit. The presented formulation only considers the subsequent hammer blow, but it is straightforward to incorporate blows resulting from any number of blows, ranging from a single blow to a full rotation of the drillbit. The authors believe that the BPI may be used in the following scenarios:

- Given a particular drillbit design, changes in drilling parameters may be recommended based on current performance. For example, if drilling at 60 RPM and a hammer frequency of 17 Hz is resulting in lower-than-expected performance, the BPI may be used to identify a new parameter combination that increases or reduces hammer blow overlap. These regions are tightly spaced, as shown in the examples above, so a change of +/- 10 RPM may change the overlap pattern significantly. Additionally, as the BPI considers downhole RPM, a transient drillstring model may be used to estimate downhole RPM in real time, such as the models proposed by (Aarsnes et al., 2019).
- When designing a drillbit, the BPI may be used to evaluate layout of inserts on the bit face to understand and quantify the overlap pattern and to make the overlap pattern sensitive to changes in RPM. Depending on the regularity in insert layout, it is possible to have a BPI that has larger or lower variability, and to widen or narrow regions of high or low value.

Future work includes (1) widening the experimental matrix for the single insert experiment to understand the effect of multiple blows in various locations, and (2) continued evaluation of field data to understand the performance of drillbits given operating parameters. In particularly, using the complex component of the BPI, a relationship between WOB and Torque may be quantified.

CONCLUSIONS

Rotary percussive drillbits exhibit a non-linear relationship between drilling parameters (RPM, Torque, Weight-on-bit and Hammer Frequency) and drilling rate. In this paper we proposed the Bit Performance Index (BPI), that is based on the shape and layout of the inserts on a bit face, and the overlap in hammer location between blows, to identify regions of higher and lower rock failure potential. This was validated with preliminary results from a single insert experiment and from initial field data. Positive agreement between the BPI predictions and observed performance indicate validity in the approach and validate the potential for the BPI to be a strong candidate for a tool to evaluate and optimize drilling parameters given a particular drillbit, and to assist in the design of future rotary percussive drillbits.

ACKNOWLEDGEMENTS

The authors would like to acknowledge the help and support of the engineers and experts at Eavor Technologies, including Willem Jordaan and Ariel Torre, for extensive feedback sessions and ideas. Additionally, we would like to thank Eavor for their support of this work and permission to publish these results. Finally, the authors would like to thank the National Science and Engineering Research Council of Canada for their funding of the Alliance Project #561118-20, Alberta Innovates of their funding of Campus Alberta Small Business Engagement Grant #212200496, and Eavor Technologies for their financial support.

REFERENCES

Aarsnes, U.J.F., Auriol, J., Di Meglio, F. and Shor, R.J., 2019. Estimating friction factors while drilling. Journal of Petroleum Science and Engineering, 179, pp.80-91.

Bu, Changgen, Yegao Qu, Zhiqiang Cheng, and Baolin Liu. "Numerical simulation of impact on pneumatic DTH hammer percussive drilling." Journal of Earth Science 20, no. 5 (2009): 868-878.

Depouhon, Alexandre, Vincent Denoël, and Emmanuel Detournay. "Numerical simulation of percussive drilling." International Journal for Numerical and Analytical Methods in Geomechanics 39, no. 8 (2015): 889-912.

Detournay, E. and Defourny, P., 1992, January. A phenomenological model for the drilling action of drag bits. In International journal of rock mechanics and mining sciences & geomechanics abstracts (Vol. 29, No. 1, pp. 13-23). Pergamon.

Detournay, E., Richard, T. and Shepherd, M., 2008. Drilling response of drag bits: theory and experiment. International Journal of Rock Mechanics and Mining Sciences, 45(8), pp.1347-1360.

Dupriest, Fred E., and William L. Koederitz. Maximizing drill rates with real-time surveillance of mechanical specific energy. SPE/IADC drilling conference. (2005)

Gerbaud, L., Menand, S. and Sellami, H., 2006, February. PDC bits: All comes from the cutter/rock interaction. In IADC/SPE Drilling Conference. OnePetro.

Han, Gang, Mike Bruno, and Maurice B. Dusseault. "Dynamically modelling rock failure in percussion drilling." In Alaska Rocks 2005, The 40th US Symposium on Rock Mechanics (USRMS). OnePetro, 2005.

Kopey, B. "Development of drilling technics from ancient ages to modern times." In 12th IFToMM World Congress, Besançon, France. 2007.

Melamed, Yuri, Andrei Kiselev, Michael Gelfgat, Don Dreesen, and James Blacic. "Hydraulic hammer drilling technology: developments and capabilities." J. Energy Resour. Technol. 122, no. 1 (2000): 1-7.

Perneder, L., Detournay, E. and Downton, G., 2012. Bit/rock interface laws in directional drilling. International Journal of Rock Mechanics and Mining Sciences, 51, pp.81-90.

Richard, T., Germay, C. and Detournay, E., 2007. A simplified model to explore the root cause of stick–slip vibrations in drilling systems with drag bits. Journal of sound and vibration, 305(3), pp.432-456.

Verma, A., and Pruess, K.: Enhancement of Steam Phase Relative Permeability Due to Phase Transformation Effects in Porous Media, Proceedings, 11th Workshop on Geothermal Reservoir Engineering, Stanford University, Stanford, CA (1986).

Wang, C.T., and Horne, R.N.: Boiling Flow in a Horizontal Fracture, Geothermics, 29, (1999), 759-772.